How kinesin-2 forms a stalk

Marija Vukajlovic[a], Hendrik Dietz[b], Manfred Schliwa[a], and Zeynep Ökten[a]
[a]Center for Integrated Protein Science Munich and Institute for Cell Biology, Ludwig-Maximilians-Universität, D-80336 Munich, Germany; [b]Center for Integrated Protein Science Munich at the Physics Department and Walter Schottky Institute, Technische Universität München, D-85748 Garching, Germany

ABSTRACT **The heterotrimeric structure of kinesin-2 makes it a unique member of the kinesin superfamily; however, molecular details of the oligomer formation are largely unknown. Here we demonstrate that heterodimerization of the two distinct motor domains KLP11 and KLP20 of *Caenorhabditis elegans* kinesin-2 requires a dimerization seed of merely two heptads at the C terminus of the stalk. This heterodimeric seed is sufficient to promote dimerization along the entire length of the stalk, as shown by circular dichroism spectroscopy, Förster resonance energy transfer analysis, and electron microscopy. In addition to explaining the formation of the kinesin-2 stalk, the seed sequence identified here bears great potential for generating specific heterodimerization in other protein biochemical applications.**

Monitoring Editor
Erika L. F. Holzbaur
University of Pennsylvania

Received: Feb 7, 2011
Revised: Aug 31, 2011
Accepted: Sep 8, 2011

INTRODUCTION

Kinesins are microtubule-associated nanomachines that harness the chemical energy from ATP hydrolysis to carry out mechanical work in eukaryotic cells. Although kinesins vary in shape, there are overarching principles concerning their molecular architecture. In addition to the catalytic motor domain, they possess a highly variable and extended stalk capable of forming monomers, homodimers, homotetramers, and, most strikingly, heterodimers. A detailed mechanistic inquiry into kinesin's overall architecture therefore is a prerequisite to the molecular understanding of how these motors accomplish their versatile cellular tasks.

One subclass of dimeric kinesins, kinesin-2, is unique in that some of its members are heterodimers with an additional accessory cargo binding subunit (Cole *et al.*, 1993). Whereas the extended stalk with its α-helical structure is involved in heterodimerization (Rashid *et al.*, 1995; Cole, 1999), the C-terminal tail is thought to interact with the accessory subunit (Wedaman *et al.*, 1996; Yamazaki *et al.*, 1996; Figure 1). None of the kinesin-2 motors seem to be able to form stable homodimers (Rashid *et al.*, 1995; De Marco *et al.*, 2003). This strong preference for heterodimerization suggests that it is of vital functional importance, but the evolutionary advantage of combining two different subunits into one functional entity is not fully understood (Brunnbauer *et al.*, 2010).

It is also unclear which regions are sufficient and which are necessary for heterodimer formation. A particularly conspicuous region is the highly charged stretch at the beginning of the stalk found in heterodimeric pairs of KRP85/95 from sea urchin, Xklp3A/B from *Xenopus laevis*, and Kif3A/3B from mouse (Rashid *et al.*, 1995; De Marco *et al.*, 2001; Chana *et al.*, 2002). Intriguingly, the two distinct polypeptide chains have complementary charges, which intuitively suggests a role in heterodimerization. The contribution of these charged regions to heterodimer formation is ambiguous, however (De Marco *et al.*, 2001; Chana *et al.*, 2002, 2005). Coimmunoprecipitation studies with Xklp3A/B from *X. laevis* revealed that the C-terminal half of the stalk is necessary to form a heterodimer, whereas truncated peptides containing the complementarily charged region did not show any tendency to heterodimerize when combined with its full-length (FL) partner (De Marco *et al.*, 2001). In contrast, elongation of the N-terminal neck residues with the complementarily charged regions in mouse Kif3A/B lead to stable heterodimeric coiled-coils in solution as demonstrated by circular dichroism (CD) spectroscopy using custom synthesized peptides (Chana *et al.*, 2005).

Here we used a multifaceted approach combining biophysical and biochemical methods to uncover the mechanism of heterodimer formation. The focus of our study is *C. elegans* kinesin-2, which separated from the line leading to its orthologues in sea urchin, frog, and mouse early in evolution. Its motor subunits, kinesin-like proteins 11 and 20 (KLP11 and 20), lack complementarily charged stretches at the beginning of the stalk. We show that heterodimerization of

This article was published online ahead of print in MBoC in Press (http://www.molbiolcell.org/cgi/doi/10.1091/mbc.E11-02-0112) on September 14, 2011.

Address correspondence to: Zeynep Ökten (zoekten@ph.tum.de).

Abbreviations used: CD, circular dichroism; CFP, cyan fluorescent protein; FL, full length; FRET, Förster resonance energy transfer; KLP, kinesin-like protein; RC, random coil tail; TEM, transmission electron microscopy; YFP, yellow fluorescent protein.

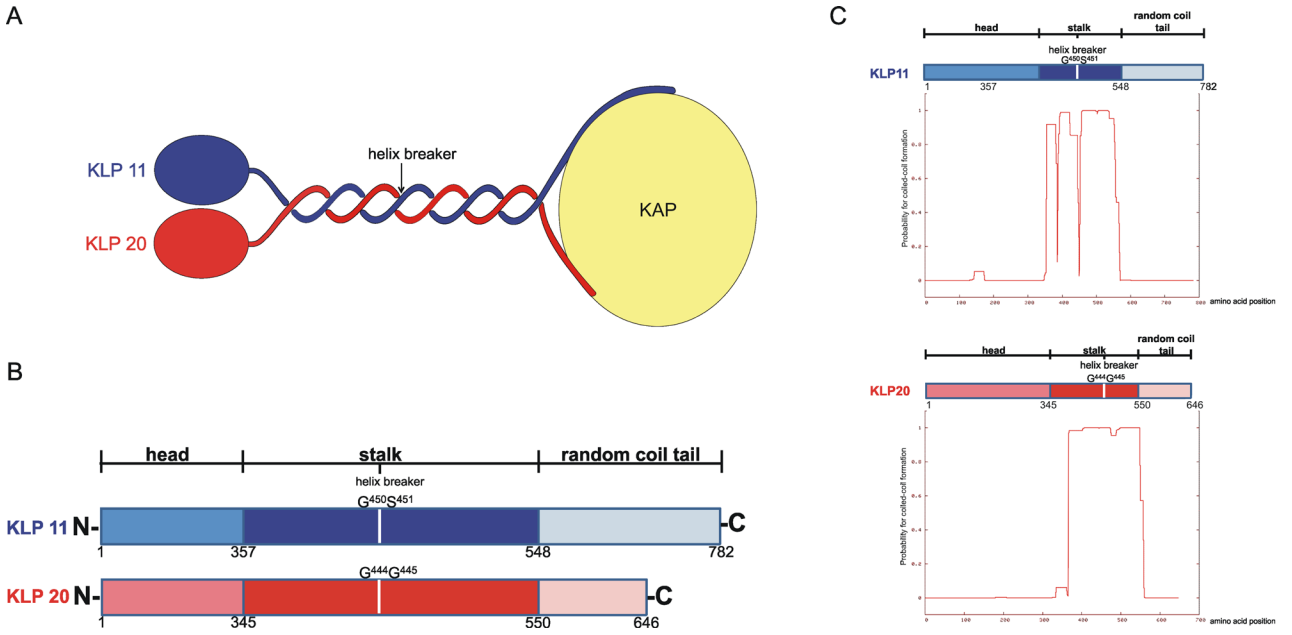

FIGURE 1: Kinesin-2 architecture. (A) Schematic overview of the *C. elegans* heterotrimeric kinesin-2. KLP11 and KLP20 form a heterodimer that C-terminally associates with the cargo binding subunit, Kinesin Associated Protein (KAP). (B) Linear maps of the two motor subunits. The head, coiled-coil stalk, and RC domains are shown together with the amino acid positions that delimit their borders. The helix breaker positions are indicated in both motor domains; they allow folding of the tail onto the head domains to autoregulate catalytic activity. (C) Coiled-coil predictions for KLP11 and KLP20. Virtually the entire stalk region in KLP11 and KLP20 is predicted to form a coiled-coil (Lupas *et al.*, 1991). The predictions are, however, limited to homodimeric coiled-coil formation.

KLP11 and KLP20 is triggered by a "seed" of approximately two heptads located at the C-terminal end of the stalk. This seed is necessary and sufficient to induce heterodimerization. Applying transmission electron microscopy (TEM), Förster resonance energy transfer (FRET), and CD spectroscopy, we demonstrate for the first time that, after being initiated by the seed, a coiled-coil is formed that spans the entire stalk in the KLP11/20 kinesin-2 motor.

RESULTS

The C-terminal half of the stalk is necessary and sufficient for heterodimerization of KLP11 and KLP20

To investigate which regions of the kinesin-2 holoenzyme are sufficient and necessary for heterodimerization, we first cut the wild-type KLP11 and KLP20 motors at the predicted helix breaker positions G451/S452 in KLP11 and G444/G445 in KLP20 (Figures 1 and 2). The helix breaker functions as a hinge-joint the flexibility of which is important for autoregulation in kinesins (Imanishi *et al.*, 2006; Brunnbauer *et al.*, 2010; Hammond *et al.* 2010). The N-terminal halves, KLP11-$N^{1\text{-}449}$ and KLP20-$N^{1\text{-}443}$, comprise the head and the stalk up to the helix breaker position (Figure 2A), whereas the C-terminal halves, KLP11-$C^{450\text{-}782}$ and KLP20-$C^{444\text{-}646}$, include the helix breaker, the C-terminal half of the stalk, and the C-terminal tail that is predicted be a random coil (RC; Figures 2B and 1C). Both halves of the stalk are predicted to form a coiled-coil (Figure 1C; Lupas *et al.*, 1991).

We used a baculovirus expression system to coexpress N-terminally Flag-tagged KLP11-$N^{1\text{-}449}$ with N-terminally hexahistidine (6xHis)-tagged KLP20-$N^{1\text{-}443}$. Likewise, the N-terminally 6xHis-tagged KLP11-$C^{450\text{-}782}$ was coexpressed with N-terminally Flag-tagged KLP20-$C^{444\text{-}646}$. Unexpectedly, despite its 13 predicted heptad repeats, attempts to copurify the truncated KLP20 with its Flag-tagged KLP11-N counterpart were not successful (Figure 2A). This is not due to failed expression of KLP20-$N^{1\text{-}443}$, as pull-down experiments with Ni-NTA confirmed the presence of 6xHis-KLP20-$N^{1\text{-}443}$ in the cell lysate (Figure 2A).

In corresponding experiments with Flag-tagged KLP20-$C^{444\text{-}646}$, its 6xHis- KLP11-$C^{450\text{-}782}$counterpart faithfully copurified (Figure 2B). According to these results only the C-terminal half of the stalk is capable of forming a stable coiled-coil by itself.

We have used size-exclusion chromatography to test the specificity and stability of this C-terminal heterodimer. The protein eluted in a 1:1 molar ratio, ruling out a possible dissociation into monomers (Supplemental Figure 1). Theoretically, the heterodimer could dissociate into monomers and subsequently form homodimers that could be separated using size-exclusion chromatography owing to their similar sizes. To rule out this possibility, we again coprecipitated the heterodimeric complex from the eluted fractions using the Flag-tag at the KLP20 subunit in a 1:1 molar ratio (Supplemental Figure 1). Taken together, these results underline that the C-terminal halves of the KLP11 and KLP20 polypeptides form a specific and stable heterodimer, as does the FL KLP11/20 (Brunnbauer *et al.*, 2010).

Heterodimerization of KLP11/20 is triggered by a seed located at the C-terminal end of the stalk

To identify the regions necessary for heterodimer formation, we systematically extended the N-terminal pair of KLP11-$N^{1\text{-}449}$ and KLP20-$N^{1\text{-}443}$ toward the C terminus. In six consecutive steps, we elongated these constructs by adding sets of at least 12 amino acids up to a chain length of KLP11-$N^{1\text{-}530}$ and KLP20-$N^{1\text{-}525}$ (Figure 3A). The longest constructs, KLP11-$N^{1\text{-}530}$ and KLP20-$N^{1\text{-}525}$, lack just three predicted heptads of the C-terminal end of the stalk (Figures 1B and 3A). Again, none of the extensions led to copurification (Supplemental Figure 2). These findings predict a distant, C-terminal region to be necessary for heterodimer formation. Including this C-terminal

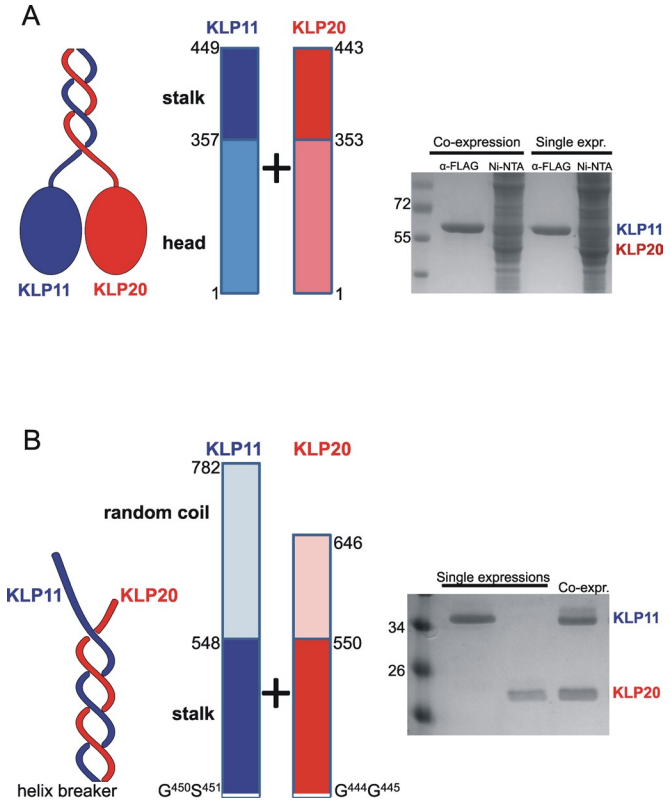

FIGURE 2: The C-terminal half of the stalk is necessary and sufficient for motor dimerization. The motor was cut at the helix breaker position. (A) Pull-down experiments of the N-terminal halves. The cell lysate was split for two different purification procedures, via anti-Flag and Ni-NTA, respectively, to ensure that both proteins are expressed successfully. The coexpression did not pull down the corresponding partner and was indistinguishable from the single expressions (single expr.). (B) Pull-down experiments of the C-terminal halves. Single expressions were with KLP11-Flag and KLP20-Flag. For coexpressions (coexpr.) KLP11-6xHis and KLP20-Flag constructs were used. Copurification of KLP11-6xHis along with KLP20-Flag via anti-Flag confirmed heterodimerization of these two polypeptides. Proteins were analyzed by SDS–PAGE. The identities of all protein bands were confirmed by mass spectrometry (LC-MS/MS). Marker protein sizes are shown in kilodaltons.

portion of the stalk (amino acids 531–548 yielding KLP11-$N^{1\text{-}548}$ and amino acids 526–550 yielding KLP20-$N^{1\text{-}550}$) led to successful copurification of both polypeptide chains (Figure 3B). This result demonstrates that the C-terminal tails (KLP11-$RC^{548\text{-}782}$ and KLP20-$RC^{550\text{-}646}$), both predicted to be random coils (Lupas *et al.*, 1991; Tripet *et al.*, 2000), are not required for heterodimerization. Indeed, coexpressed KLP11-RC and KLP20-RC did not form dimers (Supplemental Figure 3). We thus conclude that the C-terminal end of the stalk (i.e., $KLP11^{530\text{-}548}$ and $KLP20^{525\text{-}550}$) includes a trigger without which heterodimer formation of the FL KLP11/KLP20 motor is not possible.

To test whether this C-terminal region of the stalk is sufficient to form dimers on its own, and in an attempt to define the shortest sequence that is sufficient for dimerization, we elongated the RCs KLP11-$RC^{548\text{-}782}$ and KLP20-$RC^{550\text{-}646}$ by, respectively, 10, 18, and 24 amino acids of the stalk toward the N terminus. These elongations roughly correspond to the last one, two, or three heptads of the stalk (Figure 3C). Accordingly, we named these constructs RC+1, RC+2, and RC+3.

Although KLP11-$RC^{548\text{-}782}$ and KLP20-$RC^{550\text{-}646}$ did not dimerize (Supplemental Figure 3), their elongation by merely 10 amino acids toward the N terminus (RC+1) already led to copurification, as did RC+2 and RC+3 (Figure 3C). Thus, surprisingly, merely 10 amino acids of the C-terminal end of the stalk are sufficient to act as a seed for heterodimerization, requiring neither the preceding nor the following amino acids.

TEM of the wild-type kinesin-2 reveals an extended stalk

Our pull-down experiments raise questions about the extent of coiled-coil formation in the wild-type KLP11/KLP20 heterodimer. Is the seed the sole dimerization site, leaving the heads hanging on the undimerized N-terminal portions of the stalk? Or does the seed trigger the formation of a coiled-coil along the entire stalk, bringing the heads into close proximity? We used TEM to assess the molecular structure of the KLP11/KLP20/KAP heterotrimer. If the entire stalk dimerizes, the two heads can be expected to be found in close proximity to each other.

For this approach, all three wild-type protein subunits, KLP11, KLP20 and the accessory subunit KAP, were coexpressed in Sf9 cells. A Flag-tag at the C terminus of KLP20 was used to pull down a trimeric complex from the cell lysate (Figure 4, right panel).

TEM shows two globular domains at one end of a rod-shaped structure and a single globular domain at the other (Figure 4, left panel). The calculated overall length is 56.31 ± 5.9 nm (n = 183), which is in good agreement with values of other orthologues (Kondo *et al.*, 1994; Yamazaki *et al.*, 1995; Wedaman *et al.*, 1996). The two globular subunits and the single globular domain appear to be connected by a single thin shaft that possesses a certain degree of flexibility. Our micrographs thus indicate the presence of a coiled-coil structure along a significant portion of the stalk, which brings the two globular domains into proximity of 10.9 ± 1.79 nm, as measured between the centers of the globular domains. However, TEM is a relatively low-resolution method to assess the integrity of a coiled-coil, and surface interactions may affect the overall integrity of the protein. To interrogate the molecular anatomy of KLP11/KLP20 stalk more accurately, we next applied sensitive, solution-based spectroscopy.

FRET analysis confirms the close apposition of the two heads when the FL tail is present

FRET was used as a molecular nanoscale to determine whether the heads are indeed brought in close proximity by stalk dimerization, as suggested by TEM. To this end, the wild-type motor domains were replaced by either cyan (donor) or yellow (acceptor) fluorescent protein (CFP or YFP). This FRET pair is ideal for two reasons. First, an efficient FRET signal is obtained if the fluorophores are <10 nm apart (Wu and Brand, 1994; Lakowicz, 1999; Shaner *et al.*, 2005, 2007), which is the expected distance of the two heads if the stalk forms an extended coiled-coil. Second, the dimensions of the fluorophores are similar to the actual size of the kinesin heads. The KLP11 head was replaced by YFP (KLP11-YFP), and the KLP20 head by CFP (KLP20-CFP; Figure 5). The presence of two different affinity purification tags on the two polypeptide chains (KLP20-CFP-6xHis-tag and KLP11-Flag-tag) allowed the purification of heterodimers in a 1:1 molar ratio (Supplemental Figure 4). Depending on the extent of the coiled-coil, the following predictions can be made: If the coiled-coil starts at the C-terminal end and zips up the entire stalk, the two fluorophores at the N-terminus will be placed in close proximity, allowing FRET to occur. If, however, coiled-coil forms only at the C-terminal end of the stalk, FRET will be highly unlikely. Indeed, we obtained clear FRET signals for FL KLP11/20 (Figure 5, bottom panel). For the positive control, YFP and CFP were fused to

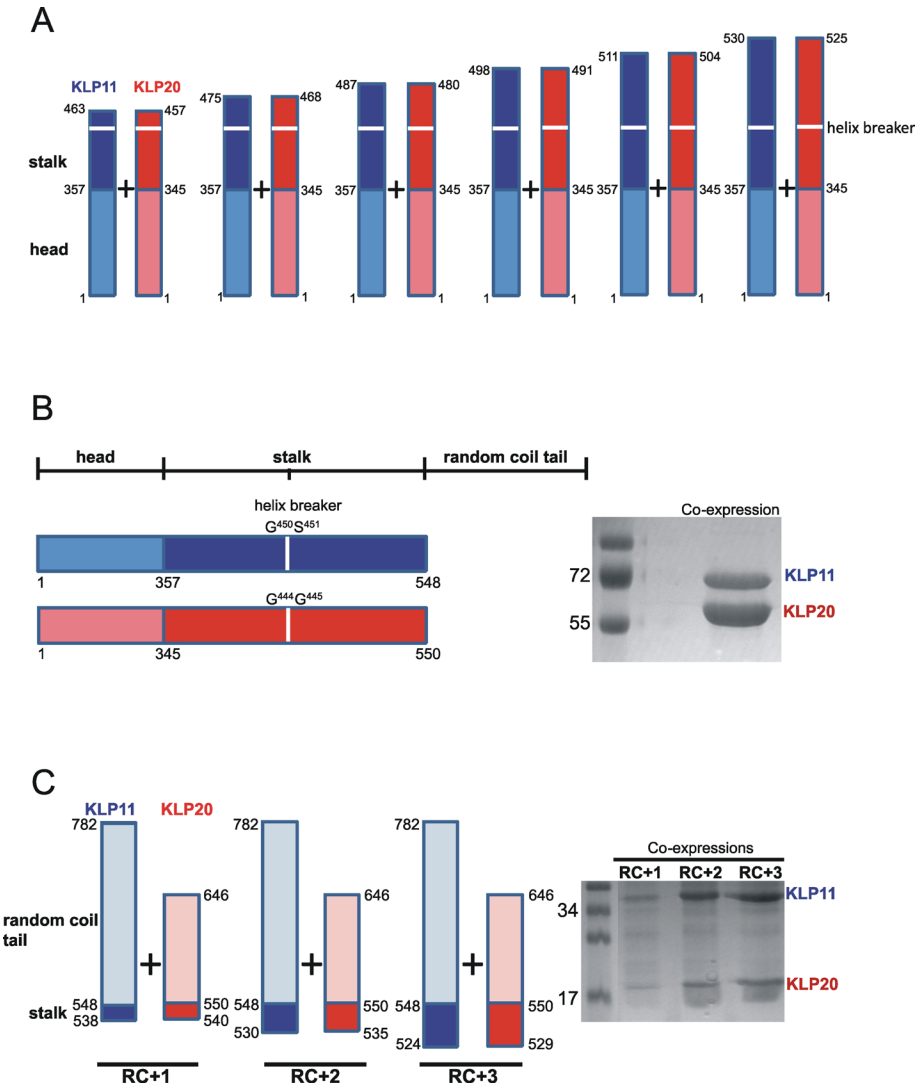

FIGURE 3: The C-terminal end of the stalk is essential for KLP11/20 dimerization. (A) The N-terminal halves of KLP11 and KLP20 in Figure 2A were elongated in six steps to include increasing numbers of residues from the stalk region. None of these extensions resulted in copurification of the coexpressed partners (Supplemental Figure 2). (B) Dimerization takes place only if the entire stalk region is included as shown schematically on the left panel. The right panel shows the successful copurification of KLP11-6xHis with KLP20-Flag via anti-Flag. (C) An elongation of the RC tails toward the N terminus by merely ten residues is sufficient for copurification via anti-Flag. Numbers correspond to the amino acid positions in the FL chain. The identities of all protein bands were confirmed by mass spectrometry (LC-MS/MS). Marker protein sizes are shown in kilodaltons.

(RC+2)-KLP11 and (RC+2)-KLP20, respectively. Because of the short dimerization sequence of 18 amino acids in the RC+2 dimer, the fluorophores must be within the FRET distance. This construct also displays an unambiguous FRET signal (Figure 5, middle panel). As a negative control we have generated a dimer consisting of FL KLP11-YFP and KLP20-RC+2 linked to CFP. This pair dimerizes via the seed sequence, but the two fluorophores are placed too far apart (>20 nm) for FRET to occur (Figure 5, top panel). After determining FRET efficiencies, approximate FRET distances were calculated to be 4.6 nm in the positive control and 4.95 nm in the FL construct (see *Materials and Methods*). No distance information for the negative control could be calculated due to the lack of a FRET signal. The lack of a positive FRET signal is conceivable given the motor's overall length of 50 nm. With a fluorophore size of 5 nm (Shaner *et al.*, 2007), the distance between the two fluorophores is expected to be more than 20 nm, which is too large to produce a positive FRET signal. Taken together, these findings demonstrate that the coiled-coil must encompass a stalk domain large enough to place the motor heads within a distance of between 3 and 8 nm, a distance range for sensitive FRET measurements with CFP and YFP (Kalab and Soderholm, 2010). These results confirm the conclusions drawn from the TEM analysis, which suggested close proximity of the head domains in the FL KLP11/20 heterodimer (Figure 4).

CD spectroscopy gauges the extent of stalk formation

To quantify the α-helical content in the stalk, we examined constructs of different lengths by CD spectroscopy. For measurements of the FL dimer the motor domains were removed, leaving the stalk and the RC tail. Other constructs analyzed were KLP11/20-C and RC+1 and RC+2 dimers (Figure 6).

The CD spectra were evaluated for double minima at 208 and 222 nm and a maximum at 195 nm, features characteristic of an α-helix (Chen *et al.*, 1972, 1974; Cooper and Woody, 1990). Interestingly, despite more than 90% of random coil, the small percentage of α-helical content in the RC+1 and RC+2 heterodimers was still detectable, and the predicted α-helical content (in percentage and amino acid residues) from the CD spectra closely matched the prediction based on sequence analysis (Figure 6 and Table 1). More importantly, the comparison of the absorption characteristics between the RC+1 to RC+2 constructs shows a significant increase in the stability of the coiled-coil (Figure 6A). Not only does the minimum at the shorter wavelength shift toward 208 nm, indicating a transition from a random coil (minimum at 197 nm), to an α-helix, but also the value at 222 nm decreases significantly (Chen *et al.*, 1974). This finding suggests once more that, although a certain length is necessary for stable dimerization, it is not more than approximately two heptads. Comparison of the CD spectra of FL KLP11/20 and KLP11/20-C offers interesting insights into the stability of the coiled-coil in the N-terminal half of the stalk. If this region forms a stable coiled-coil we expect higher amplitudes (indicative of more secondary structure) of the extrema in the FL KLP11/20 spectrum, because the coiled-coil in this dimer is twice as long as that of KLP11/20-C.

Strikingly, however, there is no apparent difference in the α-helical content in these two dimers (Figure 6B), although FL KLP11/20 is 100 amino acids longer than KLP11/20-C (Table 1). The number of predicted α-helical residues calculated from CD spectra is identical for both dimers. In the KLP11/20-C pair, however, the prediction (in percentage and number of residues) exceeds the actual number of residues of its stalk portion by 70 amino acids (Table 1). Conversely,

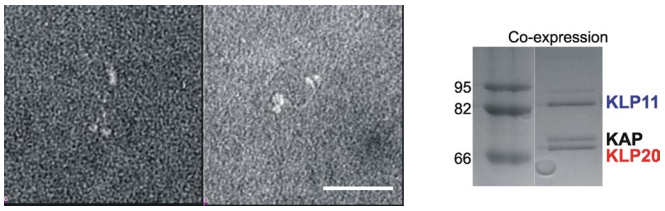

FIGURE 4: TEM indicates a long stalk and motor heads in close proximity. The micrograph shows representative images of the KLP11/20/KAP trimeric complex (n = 183). Quantification of recorded particles delivered a motor length of 56.31 ± 5.9 nm and an average distance between the centers of the motor domains of 10.9 ± 1.79 nm. Bar, 50 nm. Right panel shows the pull-down of the heterotrimeric complex used for TEM recordings via the Flag-tagged KLP20 polypeptide chain.

the CD spectrum of KLP11/20 predicts a coiled-coil that is shorter by 30 amino acids than the actual stalk sequence. Also the $[\theta]_{222}/[\theta]_{208}$ ratio, which is indicative of coiled-coil content (Zhou *et al.*, 1992; Muhle-Goll *et al.*, 1994), is higher for the KLP11/20-C pair than for FL KLP11/20 (Table 1). Furthermore, the melting temperature, T_m, is comparable for both constructs (FL-KLP11/20 T_m = 39.6°C; KLP11/20-C T_m = 39.14°C; Figure 6C), indicating no substantial gain in thermal stability in the FL dimer. Taken together, these findings suggest that the N-terminal half of the stalk forms a somewhat less stable coiled-coil.

DISCUSSION

Here we analyzed how specific heterodimerization is accomplished in *C. elegans* kinesin-2. Dimerization requires a surprisingly small seed at the C-terminal end of the stalk (Supplemental Figure 5). Without it, heterodimerization does not take place even though the rest of the stalk is predicted to form a sufficiently stable coiled-coil (Figure 1C). Thus this short sequence of approximately two heptads can be considered a genuine trigger that dictates the overall structure of the entire stalk. Such trigger sites have been found also in other proteins (Steinmetz *et al.*, 1998; Burkhard *et al.*, 2000; Araya *et al.*, 2002), although coiled-coils may fold also in their absence (Lee *et al.*, 2001). In *C. elegans* kinesin-2, however, the trigger is strictly required; its presence provokes an all-or-none response in stalk formation (Figure 3, B and C, and Supplemental Figures 2 and 5). Once triggered, the entire stalk domain forms a coiled-coil structure that brings the two motor domains in close proximity to each other.

Textbooks picture kinesins as having extensive coiled-coils in their stalks, sometimes interrupted by presumably unstructured regions. Direct evidence for this exists for kinesin-1 the stalk of which forms an α-helical coiled-coil when expressed without the head and tail domains (de Cuevas *et al.*, 1992). Moreover, even portions excised from the stalk can form stable dimers. These portions include the neck (Morii *et al.*, 1997; Romberg *et al.*, 1998; Rashid *et al.*, 2005), the N-terminal and C-terminal halves of the stalk (de Cuevas *et al.*, 1992), and the C-terminal ~80 amino acids of the stalk (Dietrich *et al.*, 2008). These findings argue against the requirement for a general trigger sequence in kinesin-1. Firm conclusions about the pathway of dimer formation (N- to C-terminal, C- to N-terminal, or multiple locations) of kinesin-1 can thus hardly be drawn.

Studies of another representative of the kinesin-2 family, Xklp3A/B of *X. laevis,* hinted at the importance of the C-terminal half of the stalk for dimerization (De Marco *et al.*, 2001). Neither the neck nor the highly charged stretch next to the neck region, which is typical for many kinesin-2 motors (but not KLP11/20), are required for heterodimer formation. The exact region was not specified but

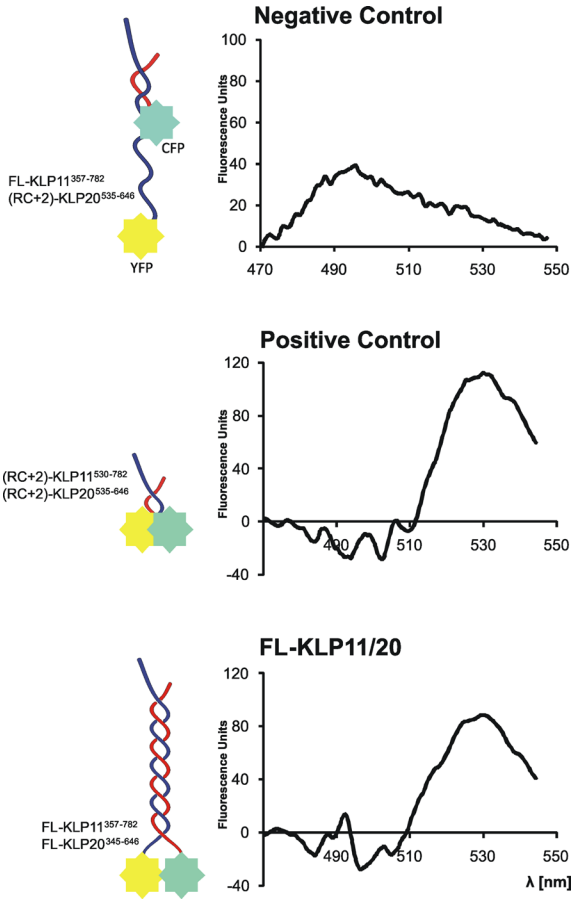

FIGURE 5: FRET analysis confirms the close proximity of the motor heads in wild-type kinesin-2. Curves represent net FRET signal obtained after subtracting signals obtained with only one fluorophore (YFP or CFP) in the CFP channel (which is also the FRET channel) from the signal obtained with the FRET pair (KLP11-YFP/KLP20-CFP) in the CFP channel. When excited with 435 nm CFP transfers energy to YFP (excitation wavelength 505 nm), which then emits with a maximum at 530 nm. FRET signal is thus visible as a peak at 530 nm. Owing to the large separation of the fluorophores in the negative control (FL-KLP11/(RC+2)-KLP20) the curve represents only the remainder of the CFP emission spectrum and no maximum at 530 nm. Positive control (RC+2)-KLP11/20 and FL-KLP11/20 all display FRET signals at 530 nm. After determining FRET efficiencies, distances between CFP and YFP were calculated to be 4.6 nm in the positive control (RC+2)-KLP11/20 and 4.9 nm in FL-KLP11/20.

was believed to encompass ~100 amino acids at the C-terminal end of the stalk (De Marco *et al.*, 2001). A trigger site was not identified, however.

What might be the reason for the different modes of dimer formation of kinesin-1 (no specific or a single trigger) and kinesin-2 (clearly specified seed)? Structurally, the major difference is that kinesin-1 forms homodimers, whereas most kinesin-2s are heterodimers. A mechanism must exist, therefore, to prefer heterodimerization to homodimerization. The latter is also possible, but exceptional (De Marco *et al.*, 2003). An ideal way indeed would be to specify a site where the two different chains have to come together first, analogous to the bottom stop and slider of a mechanical zipper that must be brought in contact before the zipper can be closed. A preference for heterodimer formation was suggested for sea urchin (Rashid *et al.*, 1995), *X. laevis* (De Marco *et al.*, 2001), and mouse (Chana *et al.*, 2005) kinesin-2. Our coprecipitation analysis delivering protein

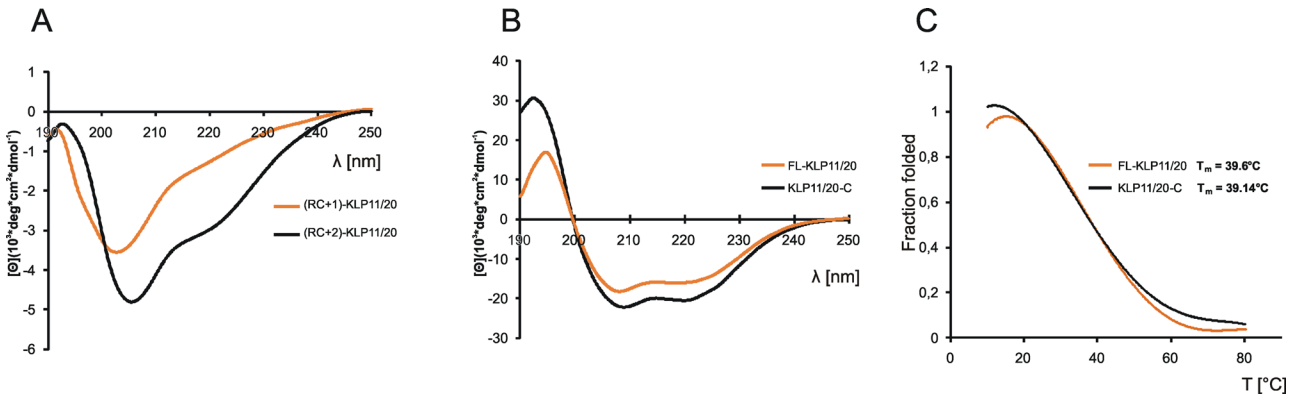

FIGURE 6: CD spectroscopy indicates an increasing coiled-coil fraction with growing chain length under native conditions. (A) Spectra of (RC+1)-KLP11/20 and (RC+2)-KLP11/20 are dominated by an RC morphology (minimum at 195 nm) due to a low α-helical content. Note the increase in coiled-coil stability from RC+1 to RC+2 achieved with only eight more amino acids. Not only does the first minimum shift toward 208 nm, but also the minimum at 222 nm becomes more prominent, both signatures indicative of increasing secondary structure. (B) KLP11/20-C and FL-KLP11/20 show typical spectra of α-helical coiled-coil with double minima at 208 and 222 nm and a maximum at 195 nm. (C) Melting curves were recorded by following the change of ellipticity at 222 nm between 10°C and 80°C. The fraction of folded protein was calculated as $f_f = ([\theta] - [\theta]_u)/([\theta]_n - [\theta]_u)$, where $[\theta]_n$ and $[\theta]_u$ represent the ellipticity values for the fully folded and fully unfolded species, respectively, and [θ] the observed ellipticity at 222 nm at any temperature. The comparable melting temperatures for KLP11/20-C and FL-KLP11/20 indicate low stability of the coiled-coil in the N-terminal half of the stalk.

bands in a 1:1 molar ratio (Figures 2B and 3, B and C) along with our CD measurements show this to be true for the *C. elegans* orthologue, too. The preference for heterodimerization becomes obvious not only because of the higher ellipticity of dimers (Supplemental Figure 6) but also their higher ratios of $[\theta_{222}]/[\theta_{208}]$ (Table 1). Furthermore, temperature-dependent CD measurements on monomeric and dimeric KLP11/20-C and FL-KLP11/20 result in one isodichroic point for monomers and two isodichroic points for dimers (Supplemental Figure 6), indicating a two-state denaturation process for monomers and a three-state process for dimers. The two states are α-helix and unfolded protein, and the three states are coiled-coil, α-helix, and unfolded protein, which again indicates favoring of heterodimerization. The difference between KLP11/20 and the other orthologues is that it lacks the charged regions following the neck, which are present in sea urchin KRP85/95, *X. laevis* Xklp3A/B, and mouse Kif3A/3B. Because KLP11/20 diverged much earlier in evolution, the charged region does not seem to be a prerequisite for heterodimerization, although it was shown to play a role in the stabilization of the neck of mouse Kif3A/3B (Chana *et al.*, 2005). Thus a contribution of the charged region to overall dimer stability cannot be generally excluded.

Our CD data also suggest that the coiled-coil stability of the N-terminal half differs from that of the rest of the stalk as indicated by the lack of a significant increase in ellipticity of FL KLP11/20 compared with KLP11/20-C. Moreover, the calculated number of α-helical residues is lower, by 30 amino acids, than the actual number contained between the neck and the C-terminal random coil (Table 1). Because 30 amino acids is approximately half of the

Peptide dimers	Chain length[a]	$[\theta]_{222}$ Observed	$[\theta]_{222}$ Predicted[b]	# of α-helical residues Included[c]	# of α-helical residues Calculated[d]	% of α-helical content Included	% of α-helical content Calculated[e]	$[\theta]_{222}/[\theta]_{208}$[f]	
(RC+1)-KLP11/20	253	–1,124	–39,275	10	8	4	3	KLP11-C	0.68
								KLP20-C	0.79
(RC+2)-KLP11/20	261	–2,790	–39,298	18	18	7	7	KLP11/20-C	0.97
KLP11/20-C	341	–19,885	–39,459	107	172	32	50	FL-KLP11	0.69
								FL-KLP20	0.74
FL-KLP11/20	434	–15,727	–39,575	205	172	48	40	FL-LP11/20	0.89

[a]Number of amino acids in KLP11 peptide including tag-residues.
[b]The predicted molar ellipticity was calculated from the equation $[\theta]_{222} = -40 \times 103 \times (1 - 4.6/n)$ (Chen *et al.*, 1974; Gans *et al.*, 1991), where n is the number of residues in the peptide.
[c]n = chain length – random coil tail – tag.
[d]The number of helical residues was calculated by multiplying the % of helical content by chain length.
[e]The (%) helical content was calculated from the ratio of the observed $[\theta]_{222}$ value divided by the predicted molar ellipticity[b] × 100.
[f]$[\theta]_{222}/[\theta]_{208}$ ratio >1 is used as an index of coiled-coil formation; the lower the ratio, the more single-stranded α-helices are contained (Zhou *et al.*, 1992; Muhle-Goll *et al.*, 1994).

TABLE 1: Summary of circular dichroism analysis.

N-terminal part of the stalk, we speculate that the discrepancy hints at an interconversion of coiled and uncoiled states of this region. Another possibility is that the coiled-coil of the N-terminal half of the stalk is not as tightly coiled as the C-terminal half although it is able to maintain a dimerized state. A lower stability of the N-terminal part of the stalk was already suggested for kinesin-1 (de Cuevas *et al.*, 1992). In general, the ends of coiled-coils were shown to be more flexible (Zhou *et al.*, 1992). Moreover, small disruptions in the flow of heptads may lead to either overwinding or underwinding of the coiled-coil (Brown *et al.*, 1996), resulting in either an increase or a decrease in helicity. Overwinding in the C-terminal half of the stalk not only would account for its higher stability but may also explain that its calculated number of amino acids exceeds the actual number by 70. Conversely, underwinding of the N-terminal half of the stalk may account for the calculated 30 amino acids less than actually present in FL KLP11/20. Support for the overwinding/underwinding suggestion comes from the melting profiles of FL-KLP11/20 and KLP11/20-C (Figure 6C). The FRET signal and the calculated distance of 4.95 nm in the FL-KLP11-20 indicate that the N-terminal half of the stalk also forms a coiled-coil, but the lack of gain in thermal stability between KLP11/20-C and FL-KLP11/20 suggests that this part of the coiled-coil is either less stable or undergoes coiling/uncoiling. The evidence for higher flexibility of the N-terminal half of the stalk may suggest that this feature is important for force generation, processivity, supertwist release, or autoregulation of kinesin's catalytic activity and may be common for heterodimeric kinesins. Whether this part of the stalk is indeed capable of switching conformations remains to be determined.

Finally, one aspect of the work described here deserves particular consideration because it points to applications beyond the study of heterodimeric coiled-coils. Because of its short length and high specificity, the nucleation seed identified here holds the promise of serving as a useful tool to induce specific heterodimerization of any two proteins. A protein sequence containing the seed can simply be fused to any pair of polypeptides by appropriate primer design. The use of such seeds for specific heterodimerization would further avoid chemical interference, such as introducing disulfide bonds, and the need for oxidizing or reducing environments, leaving the proteins in their native state and enabling protein analysis under physiological conditions. For such applications, stability of the seed heterodimer as well as mechanisms determining selectivity must be explored as it was done before for the Fos/Jun oncoprotein heterodimer (O'Shea *et al.*, 1989, 1992, 1993).

MATERIALS AND METHODS

Cloning of the protein constructs

All truncated KLP11 and KLP20 constructs for the coprecipitation experiments and CD measurements were generated via PCR from the original FL cDNA sequence (a gift from Jonathan Scholey, Cell Biology, University of California, Davis). The cloning was performed so that all KLP11 constructs were provided with either a 6xHis-tag or a Flag-tag. Tags were coded in the respective primers (forward primer for C-terminal truncations and reverse primer for N-terminal truncations). Furthermore, the respective primers contained needed restriction sites. Digested and purified PCR products were cloned into the pFastBac1 vector (Invitrogen, Carlsbad, CA), which then was used to generate the construct coding baculovirus by described and established methods (Baclulovirus-Sf9 expression system described by O'Reilly *et al.*, 1992; Invitrogen).

For the FRET constructs, fluorophores were custom synthesized by GeneScript (Piscataway, NJ). Fusion of fluorophores with the motor subunits was achieved by applying a restriction/ligation strategy.

Before performing any experiments, all vectors to be used for virus generation were sequenced, and the insert sequence was accurately checked for its correctness. After obtaining the viruses, all constructs were test expressed. The size was checked via SDS–PAGE and Coomassie staining of the polyacrylamide gel. The respective gel bands were cut out and sent for mass spectrometry analysis. After double confirmation of the constructs' correctness, they were used for further experiments.

Coprecipitation experiments

Sf9 cells were coinfected with two baculoviruses, one coding for a Flag-tagged and one for untagged or 6xHis-tagged interaction partner. After a 40-h incubation, cells were harvested and lysed (basic buffer [80 mM PIPES, 300 mM KAc, 1 mM $MgCl_2$, and 1 mM dithiothreitol] with 1% Triton X-100). Overexpressed protein was purified from the cell lysate using agarose resin coated with anti-Flag antibody (Sigma, St. Louis, MO). After 1 h of incubation, resin was washed to discard all unbound protein (basic buffer with 0.02% Tween, 500 mM KAc, and 1 mM EGTA and then with the same volume of basic buffer). Bound protein was eluted by basic buffer containing 100 µg/ml FLAG-peptides. Eluent was checked for the content of untagged/his-tagged protein via PAGE and Coomassie staining of the gel. Prospective gel bands were confirmed by mass spectrometry. When no coprecipitation of the 6xHis-tagged partner with its Flag-tagged partner was observed, Ni-NTA purification was performed to ensure that the 6xHis-tagged protein was indeed expressed. The same buffers were used, except that washing buffers contained 30 mM imidazole and elution was performed with 500 mM imidazole.

TEM

For imaging, particles were adsorbed onto glow-discharged formvar- and carbon-coated Cu400-TEM grids and then stained immediately using a 2% aqueous uranyl formate solution containing 25 mM NaOH. Imaging was performed using a Philips CM100 operated at 100 kV. Particle length and distance between globular domains were determined using ImageJ software.

In solution FRET measurements

FRET constructs were expressed and purified as described earlier in the text. All KLP11 constructs were Flag-tagged, whereas all KLP20 constructs contained a 6xHis-tag. For the actual FRET measurements, KLP11-YFP/KLP20-CFP dimers were used at a concentration of 50 nM. For the calculation of the net FRET signal, KLP11-YFP/KLP20 and KLP11/KLP20-CFP dimers were measured in the YFP and the CFP channel at a concentration of 50 nM. Whereas the measurement in the YFP channel was a mere quality control, the spectra of dimers containing only one fluorophore measured in the CFP channel were subtracted from the actual FRET measurement to obtain the net FRET signal:

$$\text{Net FRET} = (\text{KLP11} - \text{YFP/KLP20} - \text{CFP})_{\text{CFP channel}} - (\text{KLP11} - \text{YFP/KLP20})_{\text{CFP channel}} - (\text{KLP11/KLP20} - \text{CFP})_{\text{CFP channel}}$$

In the YFP channel, 505 nm was the excitation wavelength, and the emission was scanned between 500 and 550 nm with the YFP emission maximum at 530 nm. For the CFP channel, 435 nm was determined to be the excitation wavelength, and the emission was scanned in the range between 470 and 550 nm. The CFP emission maximum lies at 490 nm. In the CFP channel, not only

the CFP but also the FRET signal is detected. For each measurement, 10 spectra were recorded and averaged at a scanning speed of 10 nm/min with a PerkinElmer LS55 fluorescence spectrometer (Waltham, MA).

To calculate FRET efficiency, the following equation was applied:

$$E = 1 - (F_{da}/F_d),$$

where E is FRET efficiency, F_{da} is the fluorescence intensity of the donor in the presence of acceptor, and F_d is the fluorescence intensity of the donor in the absence of acceptor.

Approximate distances between fluorophores were calculated by the following equation:

$$r = R_0^* (1/E - 1)^{1/6} \text{ (from } E = R_0^6/R_0^6 - r^6),$$

where r is the distance between fluorophores and R_0 is the Förster radius for CFP and YFP (4.92 nm; Patterson *et al.*, 2000).

CD and transition profiles

For CD measurements, proteins were purified in 50 mM sodium phosphate buffer. Flag peptides were discarded by dialysis. CD spectra were recorded between 250 and 190 nm on a JASCO 815 (Great Dunmow, UK) spectrometer in a thermostatically controlled (20°C) quartz cell of 0.1 cm path length. Accumulation and averaging of ten spectra were performed with a scanning speed of 20 nm/min, response time of 4 s, and band width of 1 nm. Spectra were normalized to their mean residue molar ellipticity $[\theta]_{MRW}$ (deg*cm^2*dmol^{-1}).

For temperature-dependent measurements, temperature was raised from 10°C to 80°C (2°C/min). Spectra were recorded every 5°C (50 nm/min, five accumulations) 5 min after the temperature was reached.

Melting curves were recorded by following the change of ellipticity at 222 nm (θ_{222}) between 20°C and 80°C with a temperature slope of 2°C/min, a response of 16 s, and a band width of 1 nm. Fraction of folded protein at a given temperature was calculated by the following equation:

$$f_f = ([\theta] - [\theta]_u) / ([\theta]_n - [\theta]_u),$$

where $[\theta]_n$ and $[\theta]_u$ represent the ellipticity values for the fully folded and fully unfolded species, respectively, and $[\theta]$ is the observed ellipticity at 222 nm at any temperature.

Spectra were deconvoluted using Dichroweb (Provencher and Glockner, 1981; van Stokkum *et al.*, 1990; Whitmore and Wallace, 2004, 2008).

ACKNOWLEDGMENTS

We thank Renate Dombi for expert help with the cloning of most of the constructs used and checking the sequenced DNA for its correctness. We are also indebted to Thi-Hieu Ho for her help in virus generation and test expression of the truncated proteins. We thank Andrea Hohenauer for her assistance with coimmunoprecipitation assays and Ricarda Tiemeyer for her support in establishing the FRET assays. This work was supported by Deutsche Forschungsgemeinschaft SFB 863 and funds from the Friedrich-Baur-Stiftung to Zeynep Ökten. MarijaVukajlovic was supported in part by Elite Network of Bavaria's graduate program Protein Dynamics in Health and Disease. Hendrik Dietz gratefully acknowledges financial support from the Center for Integrated Protein Science and the TUM Institute of Advanced Study (both funded by the German Excellence Initiative), as well as additional support by a SFB863 Teilprojekt A9 grant funded by the German Research Society (DFG).

REFERENCES

Araya E, Berthier C, Kim E, Yeung T, Wang X, Helfman DM (2002). Regulation of coiled-coil assembly in tropomyosins. J Struct Biol 137, 176–183.

Brown JH, Cohen C, Parry DA (1996). Heptad breaks in alpha-helical coiled coils: stutters and stammers. Proteins 26, 134–145.

Brunnbauer M, Mueller-Planitz F, Kosem S, Ho TH, Dombi R, Gebhardt JC, Rief M, Okten Z (2010). Regulation of a heterodimeric kinesin-2 through an unprocessive motor domain that is turned processive by its partner. Proc Natl Acad Sci USA 107, 10460–10465.

Burkhard P, Kammerer RA, Steinmetz MO, Bourenkov GP, Aebi U (2000). The coiled-coil trigger site of the rod domain of cortexillin I unveils a distinct network of interhelical and intrahelical salt bridges. Structure 8, 223–230.

Chana M, Tripet BP, Mant CT, Hodges RS (2002). The role of unstructured highly charged regions on the stability and specificity of dimerization of two-stranded alpha-helical coiled-coils: analysis of the neck-hinge region of the kinesin-like motor protein Kif3A. J Struct Biol 137, 206–219.

Chana MS, Tripet BP, Mant CT, Hodges R (2005). Stability and specificity of heterodimer formation for the coiled-coil neck regions of the motor proteins Kif3A and Kif3B: the role of unstructured oppositely charged regions. J Pept Res 65, 209–220.

Chen YH, Yang JT, Chau KH (1974). Determination of the helix and beta form of proteins in aqueous solution by circular dichroism. Biochemistry 13, 3350–3359.

Chen YH, Yang JT, Martinez HM (1972). Determination of the secondary structures of proteins by circular dichroism and optical rotatory dispersion. Biochemistry 11, 4120–4131.

Cole DG (1999). Kinesin-II, the heteromeric kinesin. Cell Mol Life Sci 56, 217–226.

Cole DG, Chinn SW, Wedaman KP, Hall K, Vuong T, Scholey JM (1993). Novel heterotrimeric kinesin-related protein purified from sea urchin eggs. Nature 366, 268–270.

Cooper TM, Woody RW (1990). The effect of conformation on the CD of interacting helices: a theoretical study of tropomyosin. Biopolymers 30, 657–676.

de Cuevas M, Tao T, Goldstein LS (1992). Evidence that the stalk of Drosophila kinesin heavy chain is an alpha-helical coiled coil. J Cell Biol 116, 957–965.

De Marco V, Burkhard P, Le Bot N, Vernos I, Hoenger A (2001). Analysis of heterodimer formation by Xklp3A/B, a newly cloned kinesin-II from Xenopus laevis. EMBO J 20, 3370–3379.

De Marco V, De Marco A, Goldie KN, Correia JJ, Hoenger A (2003). Dimerization properties of a Xenopus laevis kinesin-II carboxy-terminal stalk fragment. EMBO Rep 4, 717–722.

Dietrich KA, Sindelar CV, Brewer PD, Downing KH, Cremo CR, Rice SE (2008). The kinesin-1 motor protein is regulated by a direct interaction of its head and tail. Proc Natl Acad Sci USA 105, 8938–8943.

Gans PJ, Lyu PC, Manning MC, Woody RW, Kallenbach NR (1991). The helix-coil transition in heterogeneous peptides with specific side-chain interactions: theory and comparison with CD spectral data. Biopolymers 31, 1605–1614.

Hammond JW, Blasius TL, Soppina V, Cai D, Verhey KJ (2010). Autoinhibition of the kinesin-2 motor KIF17 via dual intramolecular mechanisms. J Cell Biol 189, 1013–1025.

Imanishi M, Endres NF, Gennerich A, Vale RD (2006). Autoinhibition regulates the motility of the C. elegans intraflagellar transport motor OSM-3. J Cell Biol 174, 931–937.

Kalab P, Soderholm J (2010). The design of Forster (fluorescence) resonance energy transfer (FRET)-based molecular sensors for Ran GTPase. Methods 51, 220–232.

Kondo S, Sato-Yoshitake R, Noda Y, Aizawa H, Nakata T, Matsuura Y, Hirokawa N (1994). KIF3A is a new microtubule-based anterograde motor in the nerve axon. J Cell Biol 125, 1095–1107.

Lakowicz JR (1999). Principles of Fluorescence Spectroscopy, New York: Kluwer Academic/Plenum.

Lee DL, Lavigne P, Hodges RS (2001). Are trigger sequences essential in the folding of two-stranded alpha-helical coiled-coils? J Mol Biol 306, 539–553.

Lupas A, Van Dyke M, Stock J (1991). Predicting coiled coils from protein sequences. Science 252, 1162–1164.

Morii H, Takenawa T, Arisaka F, Shimizu T (1997). Identification of kinesin neck region as a stable alpha-helical coiled coil and its thermodynamic characterization. Biochemistry 36, 1933–1942.

Muhle-Goll C, Gibson T, Schuck P, Schubert D, Nalis D, Nilges M, Pastore A (1994). The dimerization stability of the HLH-LZ transcription protein

family is modulated by the leucine zippers: a CD and NMR study of TFEB and c-Myc. Biochemistry 33, 11296–11306.
O'Shea EK, Lumb KJ, Kim PS (1993). Peptide "Velcro": design of a heterodimeric coiled coil. Curr Biol 3, 658–667.
O'Shea EK, Rutkowski R, Kim PS (1992). Mechanism of specificity in the Fos-Jun oncoprotein heterodimer. Cell 68, 699–708.
O'Shea EK, Rutkowski R, Stafford WF 3rd, Kim PS (1989). Preferential heterodimer formation by isolated leucine zippers from fos and jun. Science 245, 646–648.
Patterson GH, Piston DW, Barisas BG (2000). Forster distances between green fluorescent protein pairs. Anal Biochem 284, 438–440.
Provencher SW, Glockner J (1981). Estimation of globular protein secondary structure from circular dichroism. Biochemistry 20, 33–37.
Rashid DJ, Bononi J, Tripet BP, Hodges RS, Pierce DW (2005). Monomeric and dimeric states exhibited by the kinesin-related motor protein KIF1A. J Pept Res 65, 538–549.
Rashid DJ, Wedaman KP, Scholey JM (1995). Heterodimerization of the two motor subunits of the heterotrimeric kinesin, KRP85/95. J Mol Biol 252, 157–162.
Romberg L, Pierce DW, Vale RD (1998). Role of the kinesin neck region in processive microtubule-based motility. J Cell Biol 140, 1407–1416.
Shaner NC, Patterson GH, Davidson MW (2007). Advances in fluorescent protein technology. J Cell Sci 120, 4247–4260.
Shaner NC, Steinbach PA, Tsien RY (2005). A guide to choosing fluorescent proteins. Nat Methods 2, 905–909.
Steinmetz MO, Stock A, Schulthess T, Landwehr R, Lustig A, Faix J, Gerisch G, Aebi U, Kammerer RA (1998). A distinct 14 residue site triggers coiled-coil formation in cortexillin I. EMBO J 17, 1883–1891.
Tripet B, Wagschal K, Lavigne P, Mant CT, Hodges RS (2000). Effects of side-chain characteristics on stability and oligomerization state of a de novo-designed model coiled-coil: 20 amino acid substitutions in position "d." J Mol Biol 300, 377–402.
van Stokkum IH, Spoelder HJ, Bloemendal M, van Grondelle R, Groen FC (1990). Estimation of protein secondary structure and error analysis from circular dichroism spectra. Anal Biochem 191, 110–118.
Wedaman KP, Meyer DW, Rashid DJ, Cole DG, Scholey JM (1996). Sequence and submolecular localization of the 115-kD accessory subunit of the heterotrimeric kinesin-II (KRP85/95) complex. J Cell Biol 132, 371–380.
Whitmore L, Wallace BA (2004). DICHROWEB, an online server for protein secondary structure analyses from circular dichroism spectroscopic data. Nucleic Acids Res 32, W668–W673.
Whitmore L, Wallace BA (2008). Protein secondary structure analyses from circular dichroism spectroscopy: methods and reference databases. Biopolymers 89, 392–400.
Wu P, Brand L (1994). Resonance energy transfer: methods and applications. Anal Biochem 218, 1–13.
Yamazaki H, Nakata T, Okada Y, Hirokawa N (1995). KIF3A/B: a heterodimeric kinesin superfamily protein that works as a microtubule plus end-directed motor for membrane organelle transport. J Cell Biol 130, 1387–1399.
Yamazaki H, Nakata T, Okada Y, Hirokawa N (1996). Cloning and characterization of KAP3: a novel kinesin superfamily-associated protein of KIF3A/3B. Proc Natl Acad Sci USA 93, 8443–8448.
Zhou NE, Kay CM, Hodges RS (1992). Synthetic model proteins. Positional effects of interchain hydrophobic interactions on stability of two-stranded alpha-helical coiled-coils. J Biol Chem 267, 2664–2670.